Cuprite (Cu_2O) Rydberg Excitons for Integration with Photonics

ENGR 241 Spring 2021 Final Report

Yakub Grzesik and Hope Lee

SNF Mentor: Maurice Stevens, Swaroop Kommera

Industry Mentor: Donald Gardner

Faculty Mentor: Jelena Vuckovic

Contents

Acknowledgements

We would like to extend a huge thank you to our dedicated and generous mentors, Maurice, Swaroop, and Don, and all other members of the EE241 team. We had learned about the course and reached out to learn about this opportunity rather late and are very appreciative of the guidance that we have received during this quarter. Additionally, we would like to express gratitude towards our faculty advisor Jelena, who offered the starting suggestions for this project.

Introduction

Motivation

As reported by Kazimierczuk et al the semiconductor material cuprous oxide (cuprite, or Cu_2O) is able to host giant Rydberg excitons, bounded electron and hole pairs (Scheel, Stolz, Bayer, Kazimierczuk, & Fro, 2014). Rydberg excitons, a solid-state analogue to the Rydberg atom, harbors great potential as a resource for quantum computation, information processing, and for probing exotic quantum physics, such as quantum chaos phenomena. However, for this initial report, these giant Rydberg excitons were only observed in high quality Cu_2O crystals, mined from natural sources.

An exciting development was achieved by Steinhauer et al, where highly excited Rydberg excitons were observed in an artificial Cu_2O, grown on a silicon platform via a simple, single-step thermal oxidation process. The authors furthermore demonstrated integration of Cu_2O with silicon nitride waveguides(Steinhauer et al., 2020).

Therefore, for our project, we aim to develop a process to thermally oxidize Cu and reliably grow Cu_2O for the purpose of photonics integration, and ultimately probe the promise of this platform for nonlinear and quantum optics experiments.

Background

Rydberg atoms are highly excited atoms with a hydrogen-like structure with a single excited outer electron. Like hydrogen, Rydberg atom energy levels scale as $\frac{1}{n^2}$, where n indicates the energy level. The large size of Rydberg atoms results in exaggerated properties, such as radii on the scale of μm, and interactions, such as dipole-dipole interactions that scale with n^4 (Saffman, Walker, & Mølmer, 2010). Due to these properties, Rydberg atoms are seen to be a promising platform for quantum communication, quantum computation, and many-body physics. For example, the long-range interactions between Rydberg atoms enables scalable interactions between pairs of Rydberg atoms separated at the micron scale. One application of these micron scale interaction lengths is the Rydberg blockade implemented in atomic arrays, which enable experiments like state-selective fluorescence and quantum control gates (**insert refs here)**.

Rydberg excitons therefore serve as a solid-state analogue to the Rydberg atom. Similarly, hydrogenic in structure, the exciton consists of a bound electron and hold pair and the electronic energy levels scale as $\frac{1}{n^2}$, where n indicates the energy level. When highly excited, the Rydberg exciton also displays the same

exaggerated interactions and properties as do their atomic counterpart. However, due to its solid-state nature, Rydberg excitons can also potentially be integrated with solid-state photonics and devices, such as waveguides, couplers, and resonators to allow for novel quantum and single-photon nonlinear optics experiments, and utilization as a resource for quantum communication and computation.

Film Growth Procedures

In an article by Steinhauer et al, the authors evaporated 5nm of titanium (Ti), to serve as an adhesion and barrier layer, and 700nm of copper (Cu) on silicon (Si) wafers with ~150nm of thermal oxide. The samples were then oxidized at 850°C for 1 hour in a 1mbar, artificial air environment. These conditions are motivated by the copper oxidation phase diagram, where we see that these parameter values fall within the area dominated by Cu_2O.

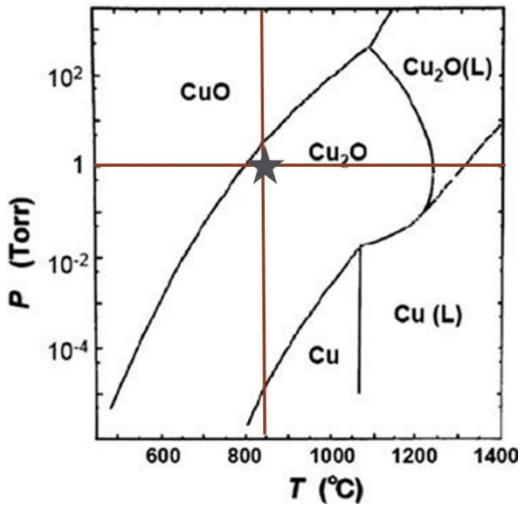

Figure 1: Phase diagram with the star marking the conditions reported by (Steinhauer et al., 2020). Figure adapted from (Amekura, Plaksin, Kono, Takeda, & Kishimoto, 2006).

Due to facility constraints and in consideration of expenses, we made a few adjustments to these reported procedures. Instead of e-beam evaporation for our metal layers, we begin with a sputtered metal stack on a silicon or silicon nitride wafer via the Lesker sputterer. For our project, we experimented with the presence and nature (titanium or tantalum) of adhesion/ barrier layers under the Cu layer, as well as with the thickness of our Cu layers (200nm or 700nm).

The main challenge proved to be the thermal oxidation of Cu layers, given that the SNF facilities was not in possession of a furnace which could simultaneously achieve all reported parameters while also accommodating Cu, considered to be a 'dirty' heavy metal, with its cleanliness standards. Therefore, we mainly focused on thermal oxidation with three different tools capable of high temperature anneals: the thermolyne, tylan-9, and Lesker sputterer.

The thermolyne is capable of a wide range of temperatures, ranging from 200°C to over 1000°C. However, the furnace has little pressure and environment control—all anneals with the tool are performed at atmosphere with surrounding ambient air.

The tylan-9, similar to the thermolyne, is incapable of vacuum or reduced pressure anneals, requiring overall pressures to be at atmosphere. However, the tool allows for control over gas composition and partial pressures, as all gases are flowed from controlled, artificial sources. The furnace is capable of reliably maintaining temperatures ranging from 300°C to over 1000°C. However, the tool is only able to be opened and loaded or unloaded when at or under 800°C, and therefore would require ramp and cool down steps if asked to anneal to temperatures greater than 800°C.

Lastly, the Lesker sputterer, despite not being a dedicated furnace tool, is able to achieve or reach values close to those we desire. The Lesker is able to maintain vacuum environments as well as flow small amounts of gases in a controlled manner. The stages can reach temperatures of around 750°C to 800°C, albeit with unstable temperature PID control. Gas control with mass flow controller parameters were not well calibrated with sample attempts, indicated by oxygen-starved samples failing to oxidize during the annealing process.

As will be discussed in later sections, we therefore referred to a larger collection of references reporting the growth of Cu_2O. We focused on two clusters of results: high temperature and low pressure growths as described earlier and reported by (Steinhauer et al., 2020), as well as low temperature, atmosphere condition growths (Choudhary, Sarma, & Gangopadhyay, 2016; Choudhary et al., 2018).

Characterization Methodology

We divided our characterizations into two main categories, material and optical. Material characterization methods informed us of the quality and nature of our oxidized films, while optical characterizations were used to probe the existence and properties of excitons within the films.

Material Characterization

Scanning Electron Microscopy (SEM)

SEM images were taken of the cleaved edges and surfaces of samples in order to visually check for complete oxidation of the film, microcrystal formation and size, surface texture, and any other potential features of note.

We mainly compared SEM images to those provided by Steinhauer et al, which reported microcrystals of around 1.5 to 2 μm in size and which grew in a cubic structure along the $\langle 111 \rangle$ direction.

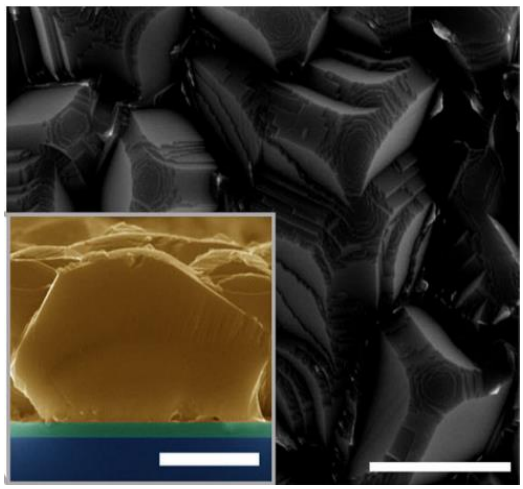

Figure 2: SEM of Cu_2O microcrystals, adapted from (Steinhauer et al., 2020). Scale bar represents 1 μm.

X-ray Diffraction Measurements (XRD)

XRD measurements were taken to determine the crystalline phases present in samples, which could be correlated to either be due to cuprite or tenorite. XRD uses Bragg's law to determine the phase composition of a material based on the intensity of x-rays diffracted into different directions by the crystalline arrangement of electrons in the sample. For characterizing our samples, we look at the reference from Steinhauer et al. in addition to extensive cuprite and tenorite literature to determine whether the cuprite phases in the (111) and (200) directions are developed. The presence of the (111) cuprite peak arising from the (111) peak in the copper film indicates an oxidation process that is formed epitaxially.

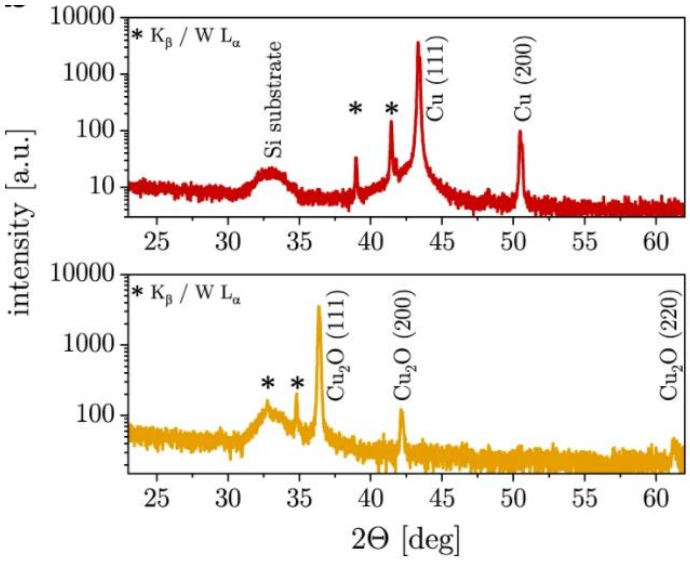

Figure 3: XRD of Cu-deposited film and Cu_2O microcrystals, adapted from (Steinhauer et al., 2020).

When doing XRD, we primarily determined if a sample had cuprite based on the magnitude of its peaks at 36.5° and 42.5°C with an occasionally weak peak at about 30°C. Tenorite, on the other hand, has signature peaks at 36° and 39°C.

All samples were characterized with grazing incidence diffraction, which characterizes only the sample, but allows for stronger signals, making characterization easier.

X-ray Photoelectron Spectroscopy (XPS)

XPS measurements were taken to verify the chemical composition of samples via peak fitting and peak area ratios. Special attention was given the Cu 2p, Cu LMM, and O 1s peaks. The sputtering capabilities of the XPS were also used to remove surface contamination or degradation from ambient conditions and investigate the chemical composition of films as a function of depth.

In order to analyze our peaks, we relied on the reference (Platzman, Brener, Haick, & Tannenbaum, 2008) which provided detailed XPS peak fitting results, although meant for characterizing native Cu oxide.

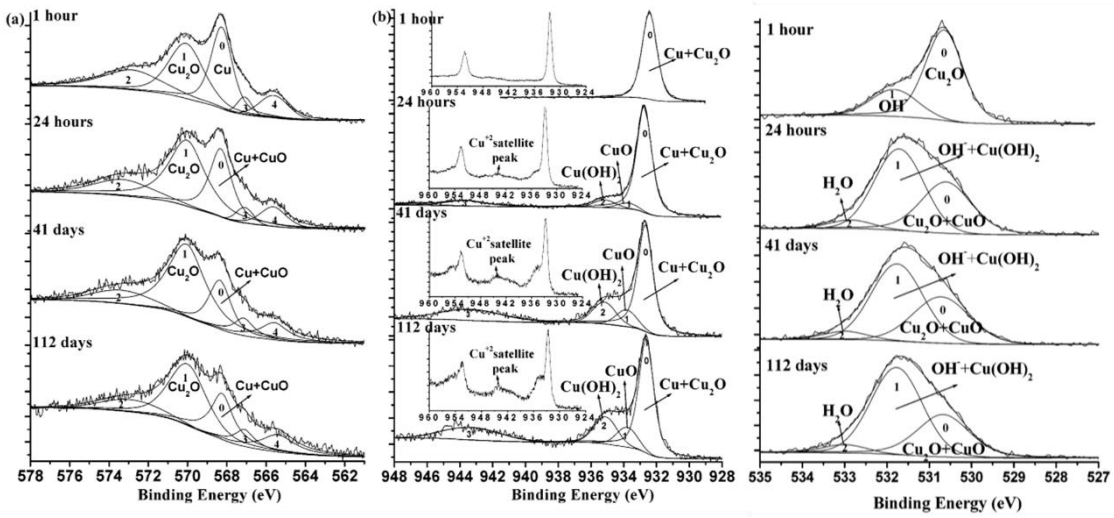

Figure 4: Peak fitting references from (Platzman et al., 2008). The leftmost diagram is of Cu LMM peak fitting, middle of Cu 2p, and rightmost of O 1s.

In addition, we also used an additional reference from the web resource “XPS Fitting” which provides a wider Cu2p spectrum, displaying the characteristic two satellite peaks attributed to CuO.

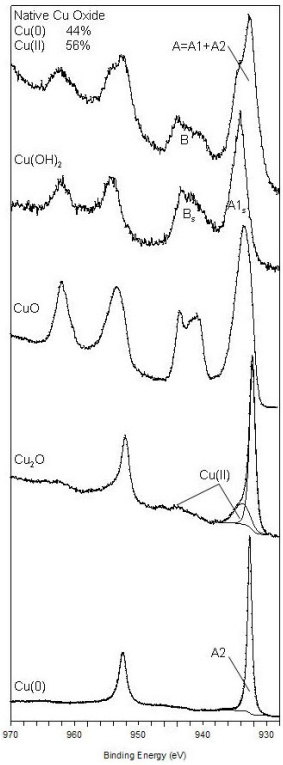

Figure 5: Additional reference which provides the characteristic shape of wider Cu2p spectrum. We see that one distinctive indicator for the CuO chemical phase is the presence of two satellite peaks.

In addition, to more reliably analyze the Cu LMM feature, we referred to the web resource XPS Simplified, which provides descriptions of the small energetic shifts of the Cu LMM feature peak.

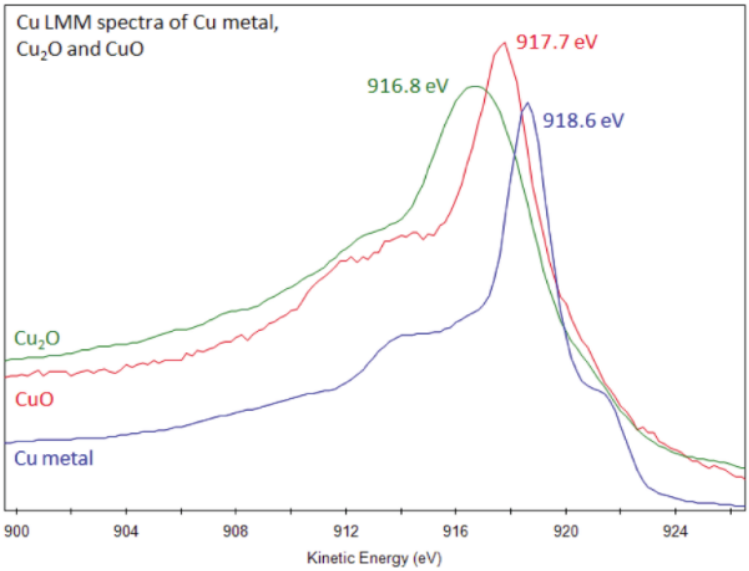

Figure 6: Figure adapted from XPS Simplified illustrating the shifts in the Cu LMM peak energy. Kinetic energy of photo- and secondary electrons can be converted to binding energy via $1486.6 - \text{kinetic energy} = \text{binding energy}$, where 1486.6 eV is the standard x-ray energy used for measurements.

Stress Measurements

The Flexus 2320 Stress Tester at SNF was used to characterize the oxidation process by observing the onset of the two phases of oxidation in copper annealing. This tool works by using dual-wavelength laser reflection off a wafer surface, which can be used to estimate the wafer's radius of curvature. The wafer is pre-characterized prior to deposition. After copper film deposition, the radius of curvature is again evaluated with laser reflection. The stress between the film and wafer is determined by evaluating the change in radius of curvature between the deposited film and the wafer's characteristics prior to deposition. The Flexus allows further characterization by including a furnace that can controllably heat up to 500°C. In contrast to prior literature, where film stress was characterized in vacuum, we anneal in atmospheric pressure to calibrate the environments achievable by the thermolyne and tylan9.

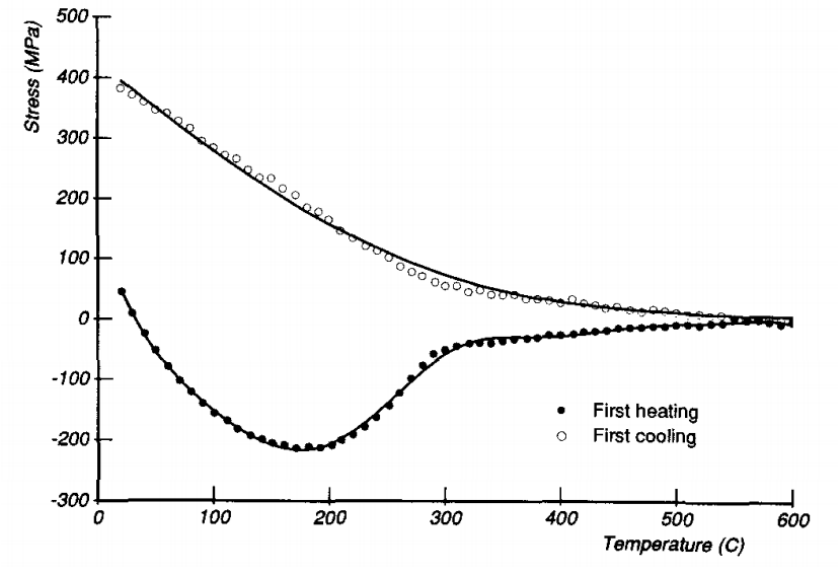

Figure 7: Figure adapted from (Flinn, 1991) that shows the stress test curve for a copper film deposited on silicon in a vacuum furnace. The difference in copper and silicon thermal expansion leads to a decrease in stress until about 200°C, after which recrystallization of the copper leads to an equilibrium towards zero stress between the wafer and deposited film.

Optical Characterization

Photoluminescence Spectra (PL)

PL was used to characterize the types of excitations produced by oxidized film. Using the setup shown schematically in Figure 8, a 532nm laser was used to excite the cuprite films. Emission was then collected into a spectrometer with a 550nm long pass filter. A spectrometer, with 150 gratings/mm for wide wavelength range spectra and with 1714 gratings/mm for high resolution narrow spectra were used to determine the intensity of emission for different transition energies. Samples were kept at either room temperature and atmospheric pressure or at 4.5K cryogenic conditions in vacuum using a Montana Cryostat in the Vuckovic Lab.

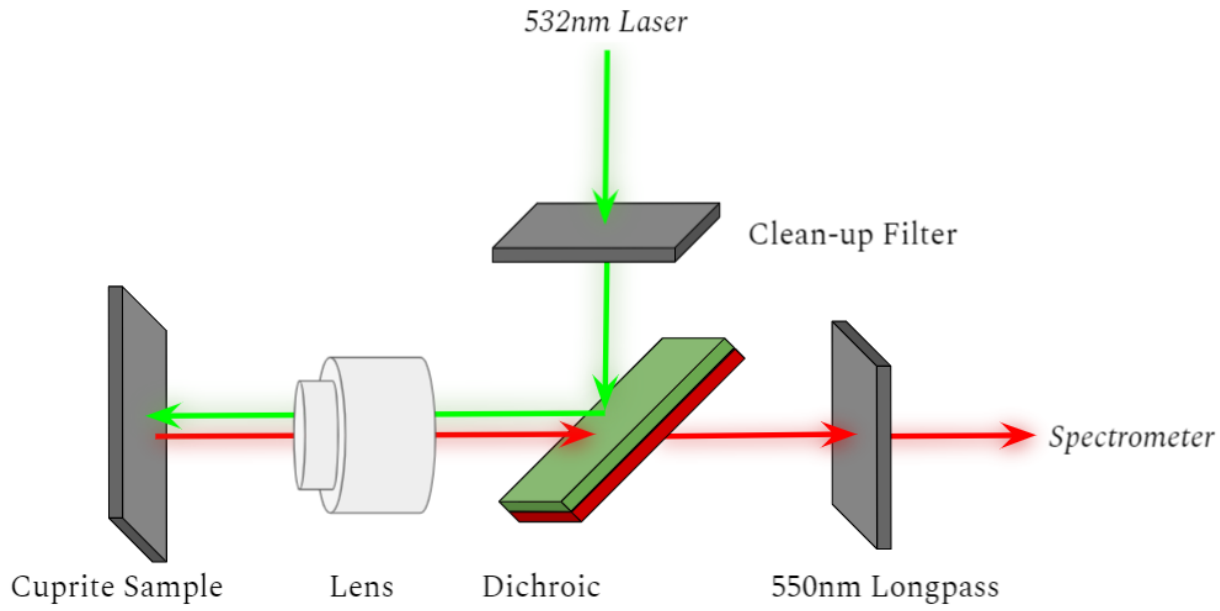

Figure 8: Schematic representation of photoluminescence setup, which uses a green laser to excite excitons on the cuprite samples we grow.

In order to characterize the films, one observes the strong peaks shown in previous literature for cuprite films, with a doublet peak structure at about 2.0 eV in room temperature and atmosphere conditions. This peak is attributed to free exciton emission, with the doublet arising from different phonon-assisted recombination mechanisms. The lack of emission in energies attributed to vacancies in copper and oxygen in previous literature suggests high crystalline quality free of defects.

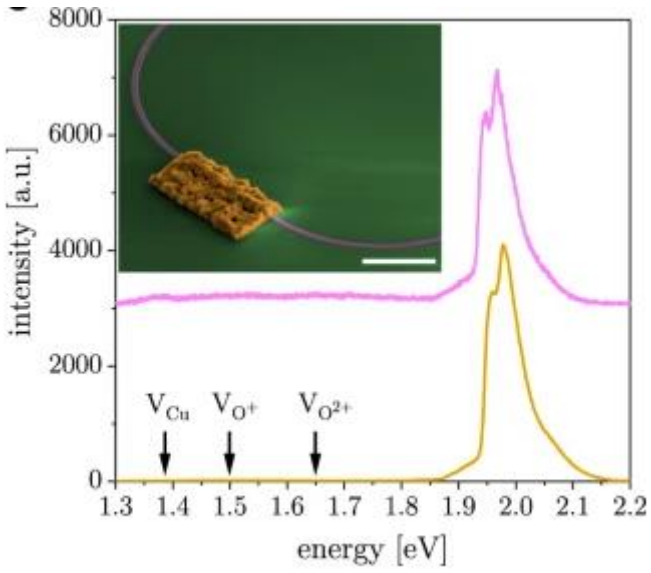

Figure 9: Room Temperature PL of Cu_2O microcrystals both from direct collection on microcrystals (orange line) and from coupled waveguides (magenta line), adapted from (Steinhauer et al., 2020).

In order to observe Rydberg excitons, which have narrow lines, it is necessary to conduct PL experiments at cryogenic temperatures. Our Montana Cryostat in the Vuckovic lab can reach 4.5K sample temperatures with approximately 2.11mK temperature stability. Steinhauer et al. report the spectrum shown in Figure 10 at 1.5K conditions. While not attainable under the Montana Cryostat, these conditions can be recreated in the Vuckovic's Attodry chamber for future sample characterizations. Under these conditions, the np orbital series of Rydberg excitons up to n=6 are visible with distinct peaks at energy levels following the n^{-2} Rydberg series. At these separations, a high resolution grating spectrometer is required. In order to combat power broadening of these narrow lines, low excitation powers on the order of 50µW were used.

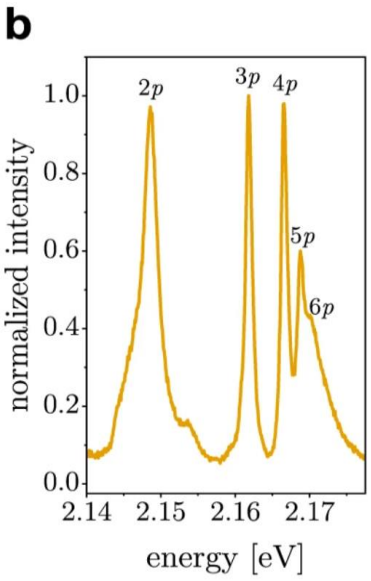

Figure 10: Cryogenic Temperature PL of Cu_2O microcrystals demonstrating the np Rydberg series of Rydberg excitons, adapted from (Steinhauer et al., 2020).

Results

Stress Test Annealing

For general characterizations of annealing growth, we were able to produce the following growth stress-curves for annealing up to 400°C. The sample produced is 700 nm of Cu sputtered onto a 5nm adhesion layer of Ta on top of a Si wafer. Like in the vacuum annealed Cu film (Figure 7) the silicon wafer expands at a different rate than the copper film, leading to decrease in stress. The copper film follows a similar trajectory as in vacuum until 250°C. At this point, an oxidation procedure begins, leading to a change in the crystalline structure of the copper film. The oxidation of copper into cuprite leads to a change in the stress curve, as cuprite has a different crystal volume than Cu. This change in stress continues in a familiar parabolic trajectory until about 320°C. At this point, a sudden change in the slope indicates the growth of a new phase, which has a sharper decrease in the stress as a function of temperature. Literature suggests that these two points are due to the onset of cuprite and tenorite, respectively. Thus, the stress test curve corroborates the growth conditions we chose at atmospheric pressure to produce cuprite.

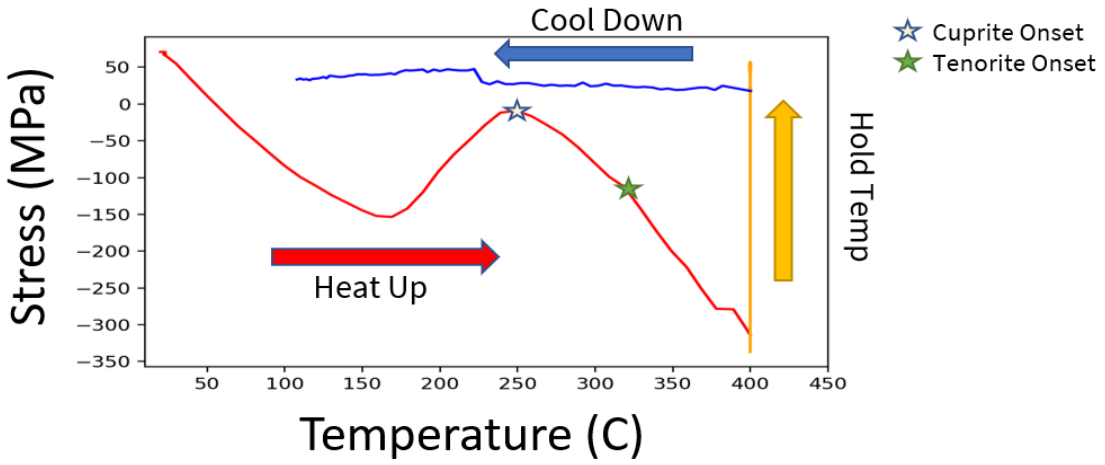

Figure 11: Stress test of a copper film on silicon undergoing the atmospheric annealing process up to 400°C. 5nm of Ta were sputtered onto a Si wafer as an adhesion layer. 700nm of Cu was sputtered on top of the adhesion layer and is the primary surface undergoing annealing.

A second stress test was conducted on a wafer with a 5nm Ti adhesive layer. In this stress test sample, we set the maximum temperature to be 280°C to be squarely in the cuprite growth phase region. Holding the sample at this maximum temperature allowed us to characterize the approximate time for oxidation based on how long it took the stress curve to reach equilibrium stress between the cuprite film and the silicon wafer. Differences in this stress test measurement may have also arisen due to the use of a Ti layer instead of a Ta one. The data below may suggest that the oxidation process for cuprite takes longer than that of tenorite, as we still see some large degrees of compressive stress in the film during the cooldown process, which happened after about 2 hours of holding the annealing temperature.

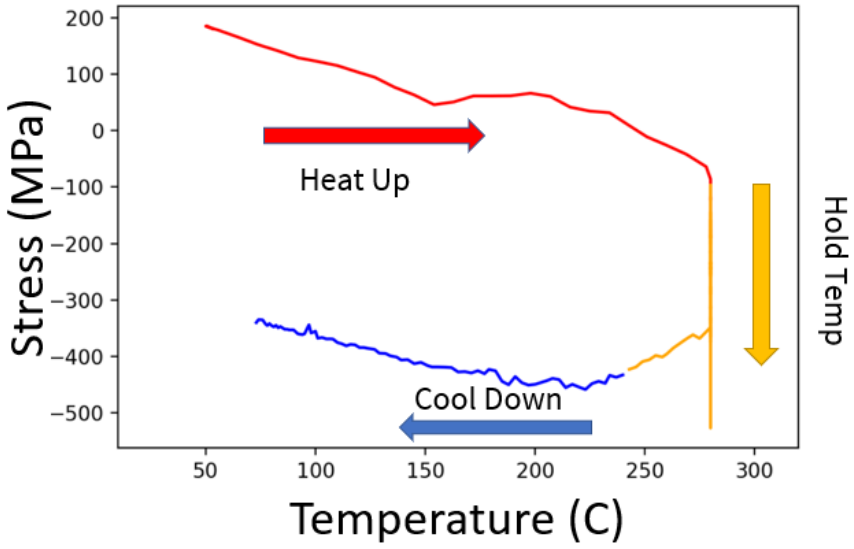

Figure 12: Stress test of a copper film on silicon undergoing the atmospheric annealing process up to 280°C. 5nm of Ti were sputtered onto a Si wafer as an adhesion layer. 700nm of Cu was sputtered on top of the adhesion layer and is the primary surface undergoing annealing.

High Temperature Growth

For high temperature growths, we were able to achieve CuO samples with microcrystalline structure.

One representative high temperature sample which demonstrates said crystalline quality was grown in the tylan-9 at 800°C for 3hr with artificial air. A SEM image of the sample is given below, illustrating clean microcrystals around 1.5 to 2 μm in size.

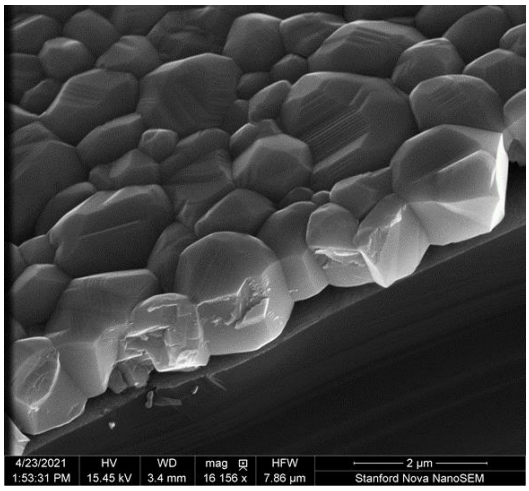

Figure 13: Sample grown at high temperatures which demonstrate clean CuO microcrystals. The sample was processed with the tylan-9 furnace at 800°C for 3hr in artificial air.

XPS spectra, specifically of the Cu 2p peaks and the Cu LMM features, of this representative sample provided evidence of its tenorite nature. We first present below a wide Cu2p spectrum which illustrates the distinctive satellite peaks which indicate a CuO chemical phase.

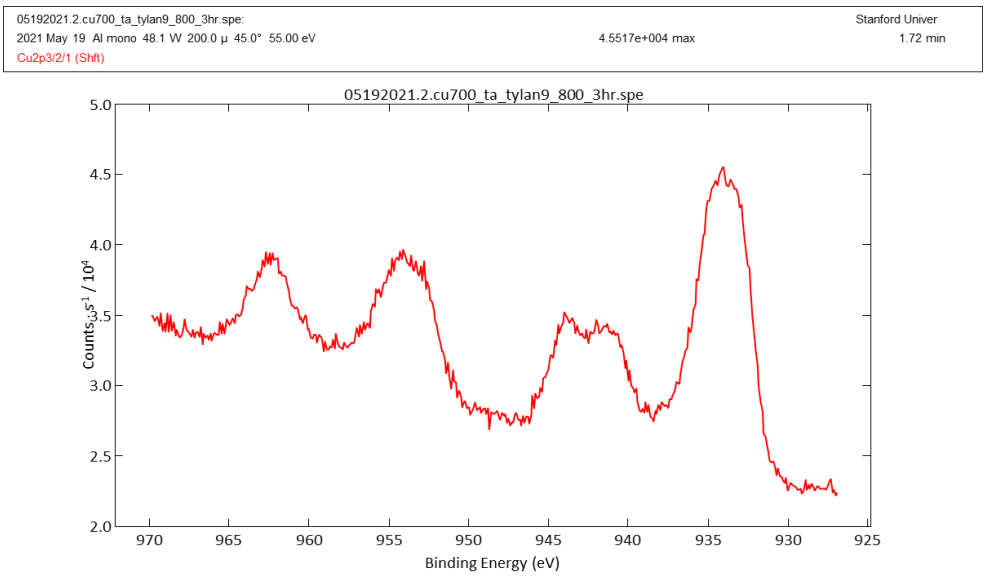

Figure 8: Wider Cu 2p peak spectrum, showing 2 satellite peaks which indicate the existence of the CuO chemical phase.

It is possible to fit the rightmost peak feature of the Cu2p spectrum in order to determine the ratio of CuO and Cu_2O phases in the film; the peak fitting is presented in the next figure.

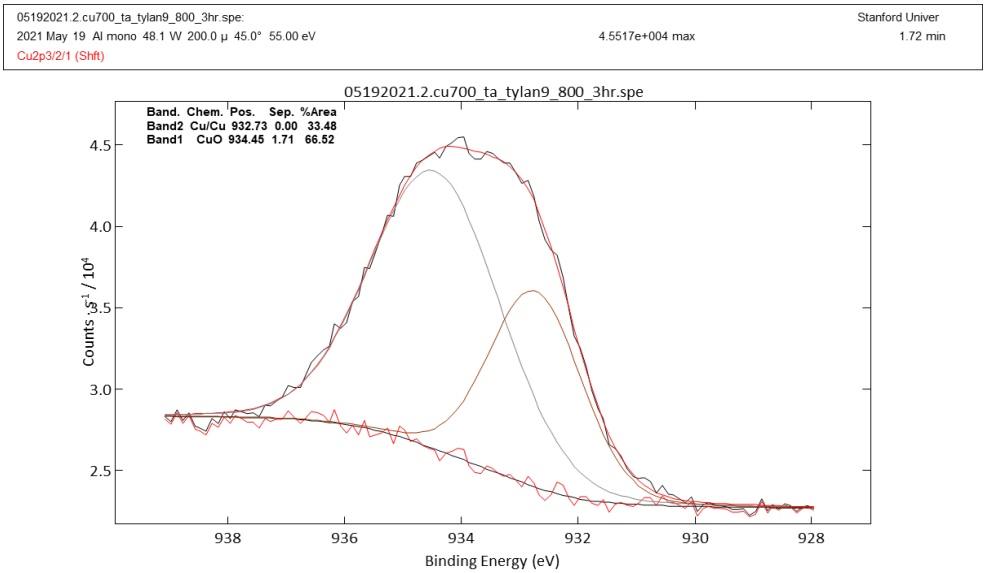

Figure 9: Peak fitting of the rightmost peak feature from the Cu2p spectrum. We see that that the Cu_2O to CuO ratio is around 1 to 2. The presence of Cu_2O may be attributed to surface degradation and oxidation due to ambient conditions. Nonetheless we see that the CuO phase dominates in the film.

In addition to investigating the Cu2p peak features, we can also try to further confirm our conclusions regarding the nature of the film by referring to the Cu LMM feature, as we present below. For the Cu LMM feature, given the complicated peak fitting scheme, we mainly check the feature maximum against those reported for various Cu phases.

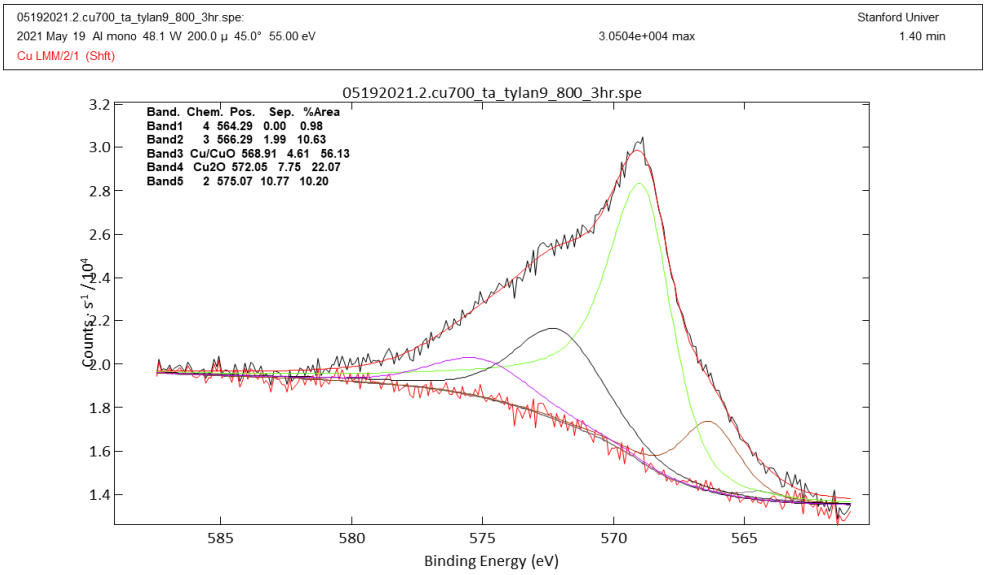

Figure 10: Peak fitting of the Cu LMM feature. We identify that the maximum of this feature is at around a binding energy of 568.9 eV, which corresponds to a kinetic energy of around 917.7 eV, exactly as expected for a CuO dominant phase material.

XRD of the high temperature growth sample further solidly identifies the sample as a tenorite microcrystal. None of the signature cuprite peaks are present. Instead, the tenorite phase peaks from (002) and (111) phases are dominant. The relative prevalence of the (111) peak indicates epitaxial growth between the (111) Cu phase and the (111) CuO phase. Furthermore, the large peak at 45° suggests strong oxidation and potential diffusion of the Ta barrier layer, leading to a strong detection of Ta_2O_5 peaks present on the sample surface.

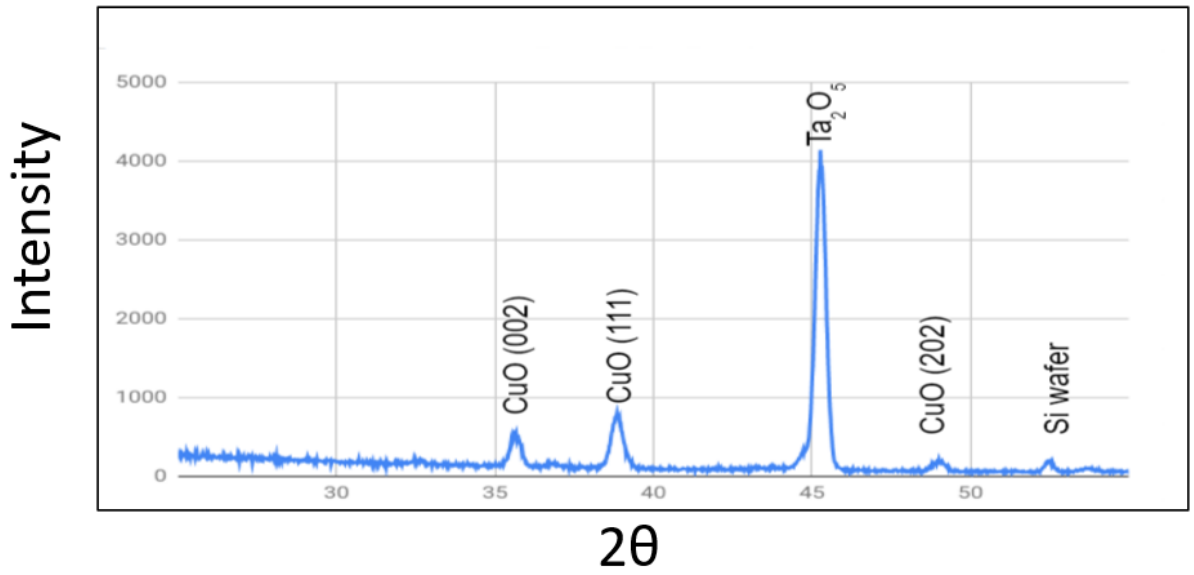

Room temperature PL was performed on this sample, but the weak signal at room temperature did not indicate or reveal any spectral features relevant to the creation of Rydberg excitons. Previous literature on photoluminescence studies of PL for tenorite suggest that most of its features such as the bandgap are located below 500 nm, which are not possible to excite with a 532nm laser.

Low Temperature Growth

For low temperature growths, we were able to achieve Cu_2O samples of lower crystallinity.

The representative sample we will use to present our characterizations was processed for 24hr at atm pressure and conditions at 250°C in the Thermolyne furnace. The lower crystallinity can be seen the SEM image provided below.

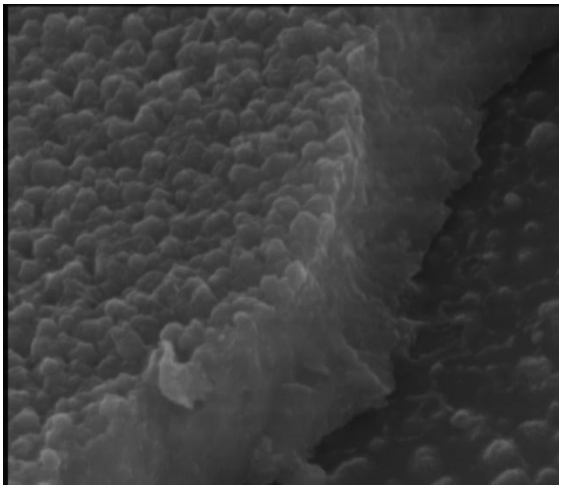

Figure 11: Sample grown at lower temperatures, namely 250°C for 24hr in the Thermolyne, displays 'cauliflower'-like textures rather than clean microcrystals as in the high temperature sample presented previously.

We can process with XPS characterizations for the low temperature sample, starting with the Cu2p spectrum and then fitting the rightmost peak as we did so previously for the high temperature samples. The wide range spectrum is presented first, showing how surface degradation and native oxidation from the ambient conditions can lead to muddling between the CuO and Cu_2O signals with the presence of satellite features. We are able to detangle the two through peak fitting to see that the Cu_2O phase dominates in the material.

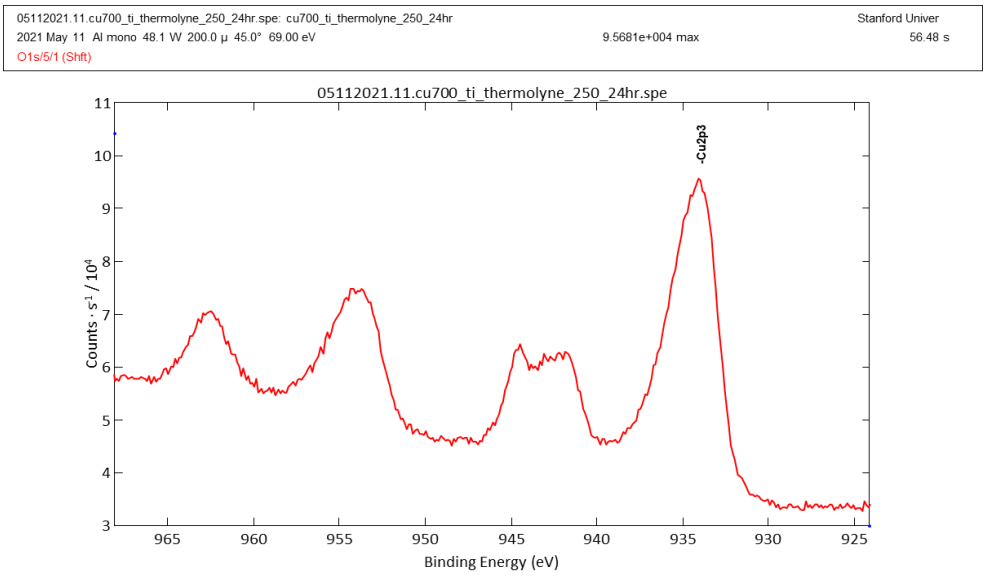

Figure 12: Cu2p spectrum for our representative low temperature growth sample. Despite the material consisting nearly purely of Cu_2O phase, as we determine from further characterizations, the initial Cu2p spectrum displays characteristic CuO satellite peak features.

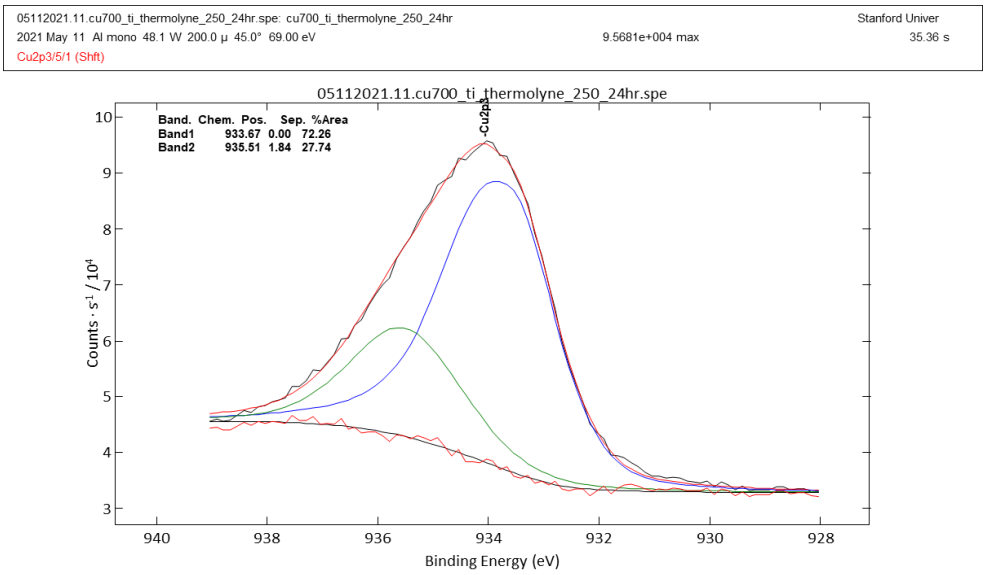

Figure 13: Peak fitting for the rightmost peak of the Cu2p spectrum. The ratio of Cu_2O to CuO phases was measured to be around 3 to 1. Similar to the high temperature sample, the presence of the CuO phase is most likely to be attributed to surface degradation and native oxide formed under ambient conditions.

To further verify that surface degradation has taken place, we can turn to the O1s peak features, as presented below. The strong presence of a water peak suggests that surface contamination has taken place between sample fabrication and measurement.

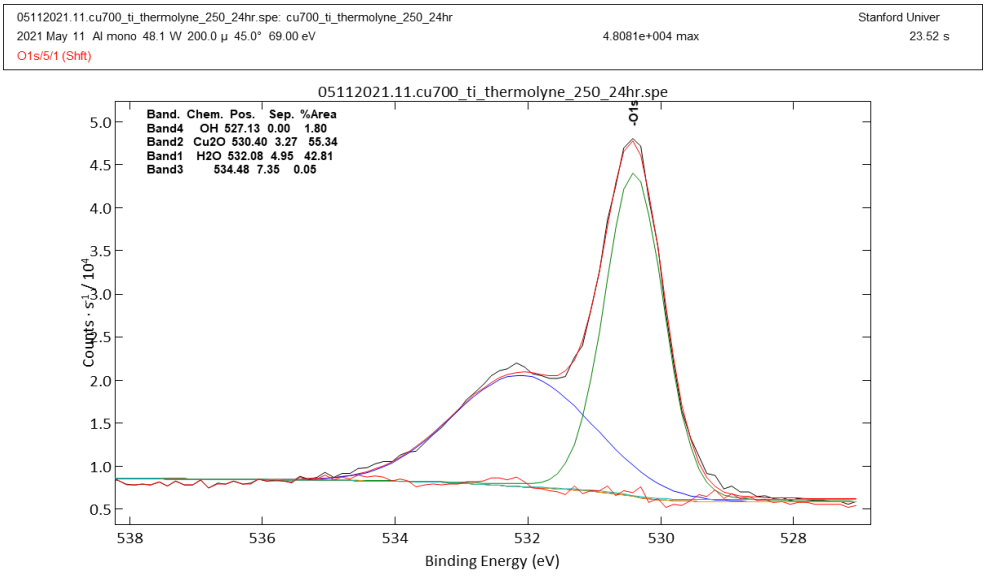

Figure 14: Peak fitting of the O1s peak for the low temperature sample. As we can see there is strong evidence for the presence Cu_2O, but also a significant signal for water, indicating surface contamination and degradation.

Therefore, to even more closely investigate this sample and confirm the existence of bulk Cu_2O, we sputtered around 200nm of the surface using the XPS surface gun, effectively removing the surface layers. However, it is to be noted that although sputtering allows for probing the bulk of the material film, the energy Ar + ions used for the process simultaneously reduces metal compounds. Therefore,

Cu^{2+} could be reduced to Cu^{1+} (oxidation state of CuO to Cu_2O), and Cu^{1+} to Cu (oxidation state of Cu_2O to Cu). Therefore, after sputtering, the Cu features are not longer as reliable for chemical phase identification, and instead we rely on both the Cu peak features and the O1s peak.

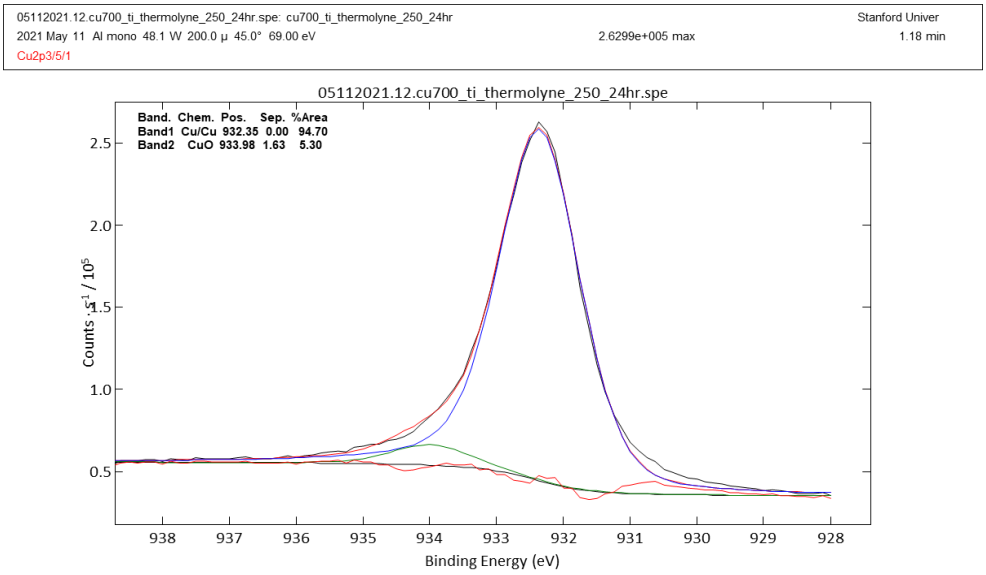

Figure 15: Cu2p spectrum, rightmost peak fitting after sample sputtering. The peaks fitting seems to suggest a high purity Cu_2O phase, but cross reference is required since Cu^{2+} reduces to Cu^{1+}

However, since reduction does not happen to the oxygen involved in the compound, we are able to cross reference the after sputtering Cu2p peak fits with the O1s peak fit to determine the chemical phases present.

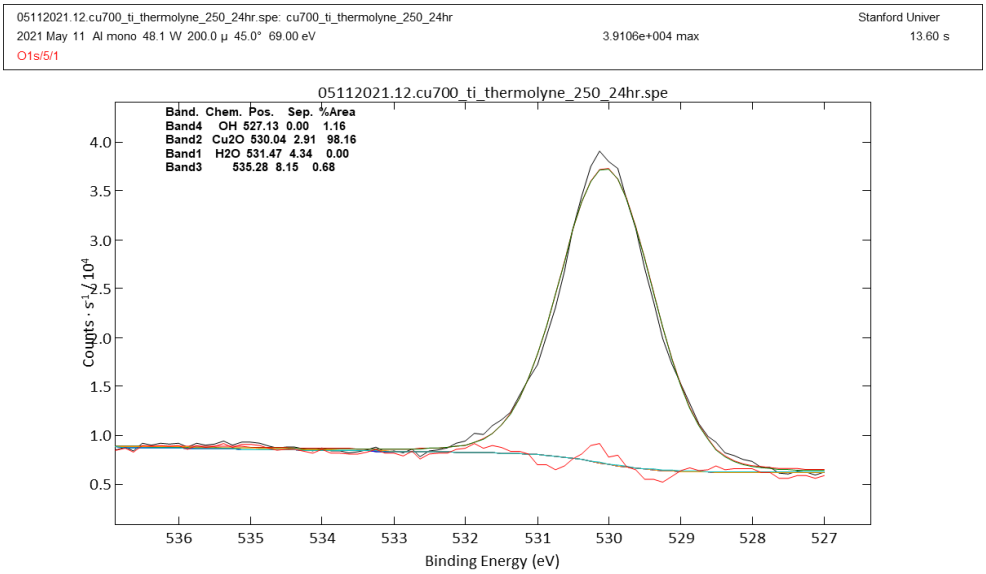

Figure 17: O1s peak fitting, after sample sputtering. As we can see, the previously strong H_2O signal has been eliminated through sputtering, and we see a high purity single Cu_2O phase O1s peak. In conjunction with the Cu2p peak fitting, we can therefore conclude that it is very likely the bulk of the film Cu_2O.

XRD was performed on this sample, producing the spectrum below. In it, we see strong evidence that the film is predominantly cuprite. The (111) peak and its intensity supports epitaxial growth from the Cu (111) phase to the (111) cuprite phase. The potential (111) CuO peak is present, but it is significantly weak enough to indicate a successful cuprite growth. The lack of other CuO peaks corroborates this.

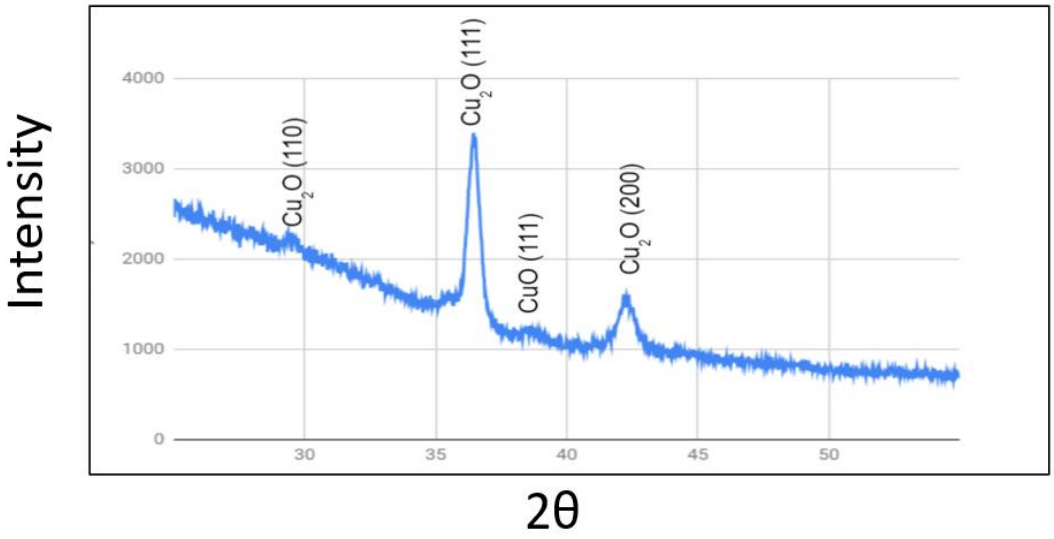

Figure 18: XRD spectrum of low temperature annealed sample in the thermolyne. The signature peaks of the cuprite phase dominate, indicating a cuprite film.

Since this film exhibited promising cuprite properties in chemical characterization, we proceeded with optical studies by performing PL at room temperature and cryogenic conditions. Unless otherwise noted, a 1mW excitation power was used with 30s integration time.

The room temperature PL, shown below for the low temperature annealed sample had a weak signal, but was comparatively stronger than that of the tenorite film. There is a doublet peak structure located around 560nm and 570nm, but this is in contrast with the previously referenced literature, which suggests a doublet structure at 620nm and 635nm. This difference may be due to the different crystalline structure in our sample compared to that of literature. While this spectrum also indicates little presence of the vacancy defect emitters, it does not necessarily suggest any expected Rydberg exciton emission at low temperatures.

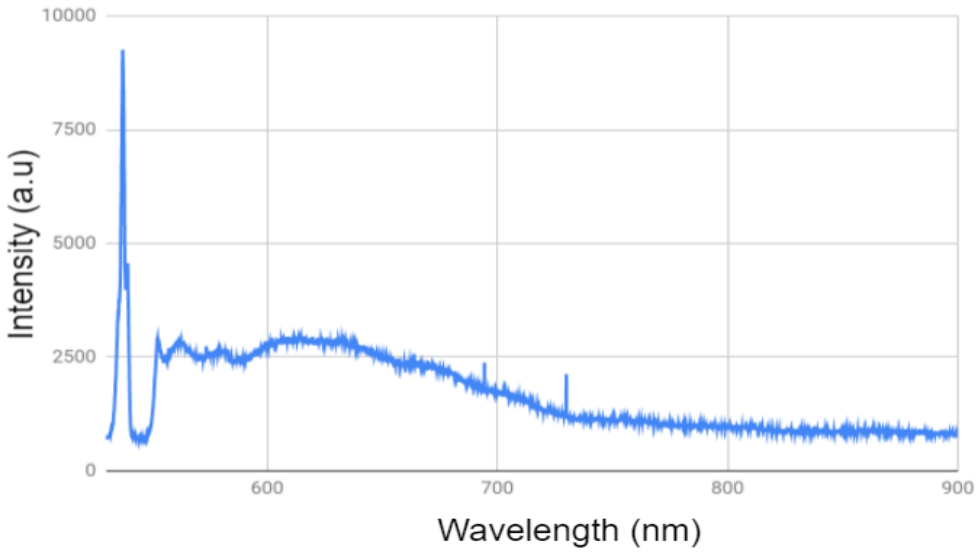

Figure 19: Room temperature PL spectrum of low temperature annealed sample in the thermolyne. There are slight peaks around 560nm and 570nm, indicating a weak doublet structure, but they are blue-shifted compared to the referenced studies on cuprite microcrystals.

The spectrum below, taken broadly at cryogenic temperatures demonstrates defect emission centered around 1.75 eV, which agrees with literature, but is missing the orthoexciton emission reported for natural and synthetic cuprite crystals reported around 2.05eV. This may be due to orthoexcitons requiring millikelvin temperatures to become observable or due to lack of crystal quality in our low temperature annealed sample. This suggests that we would need improvements to both the sample quality and cooldown temperatures achievable by our setup in order to better characterize the films.

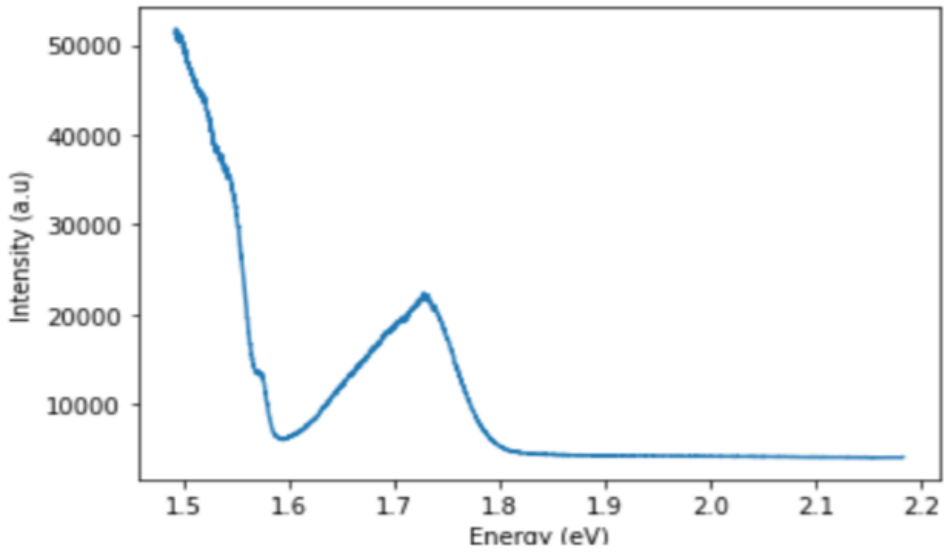

Figure 20: 4.5K PL spectrum of low temperature annealed sample in the thermolyne. There is a large peak centered at 1.75 eV which has been reported as defect-related emission in previous literature. However, orthoexciton emission, usually reported around 2.05 eV for millikelvin temperatures is absent.

A higher-resolution spectrum was taken centered at the energies where previously reported Rydberg excitons have been found. The resulting data is plotted below. We see a broad peak centered at a slightly higher energy than previous reports, but the emission is difficult to resolve due to grating parameters and power broadening. Lower excitation power would be required to resolve potential peaks, but due to lacking signal strength, this would require prohibitively long integration times.

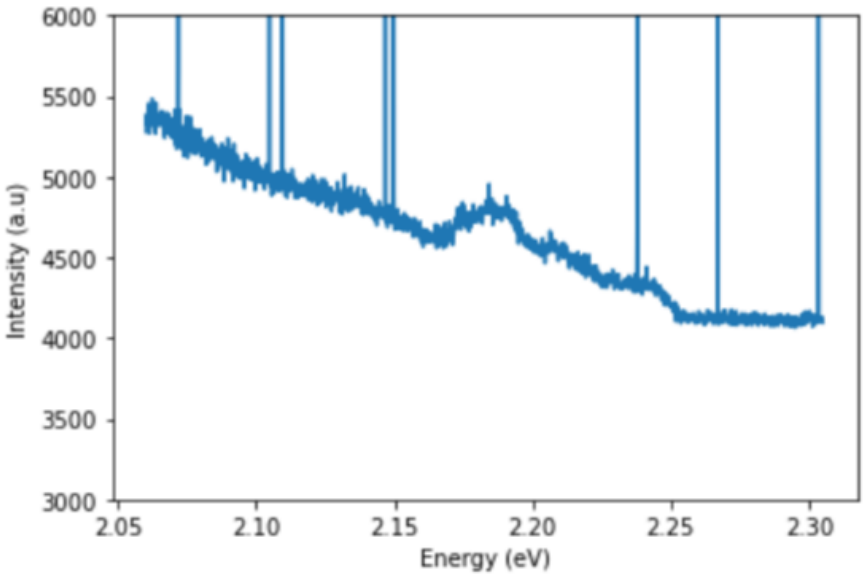

Figure 21: 4.5K PL spectrum of low temperature annealed sample in the thermolyne with 1714 gratings/mm grating parameter. The emission near Rydberg excitation energies suggests some form of excitation potentially induced by Rydberg transitions, but limits in resolution and signal power prevent further investigation, most likely due to lacking microcrystal quality. Large spikes of signal above 6000 counts are due to cosmic ray spurious noise.

Low Temperature Growth-SiN wafer Sample

One final sample we considered from the low-temperature growth batch was a sample of 700nm Cu with 5nm of Ti grown on a SiN wafer. This sample was made to test adhesion on SiN, which would be the platform that we ultimately plan to grow waveguide components. The deposited film was annealed in the tylan9 at 300^{o}C for 1 hour. The XRD spectrum, produced below shows promising growth of cuprite phases, albeit with some slight tenorite peak presence

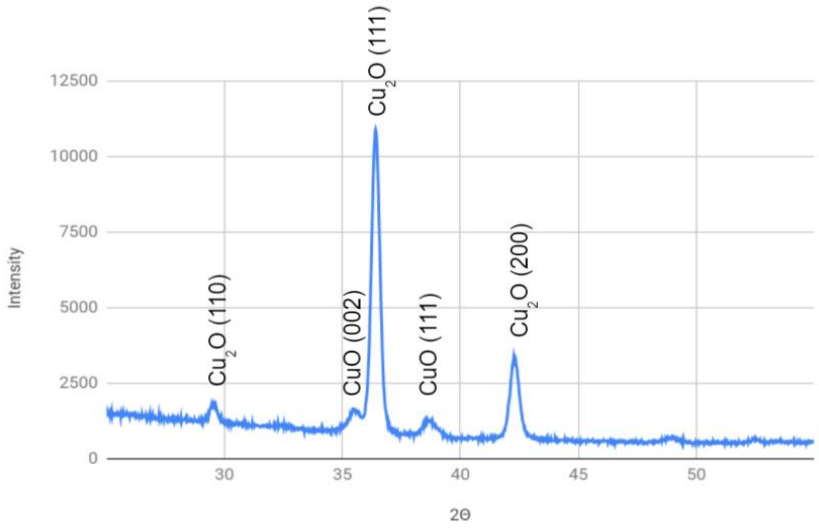

Figure 22: XRD spectrum of low temperature annealed sample in the tylan9 deposited on SiN. The signature peaks of the cuprite phase dominate, indicating a cuprite film. There is a trace amount of tenorite present, indicated by the labelled XRD peaks.

At cryogenic temperatures, this sample demonstrated promising PL features, with a narrow emission band slightly blueshifted by about .05 eV from previously reported Rydberg series emitters in cuprite. Although this sample had sharper contrast than the other low temperature-annealed sample, it also suffered from requiring too low excitation powers to resolve.

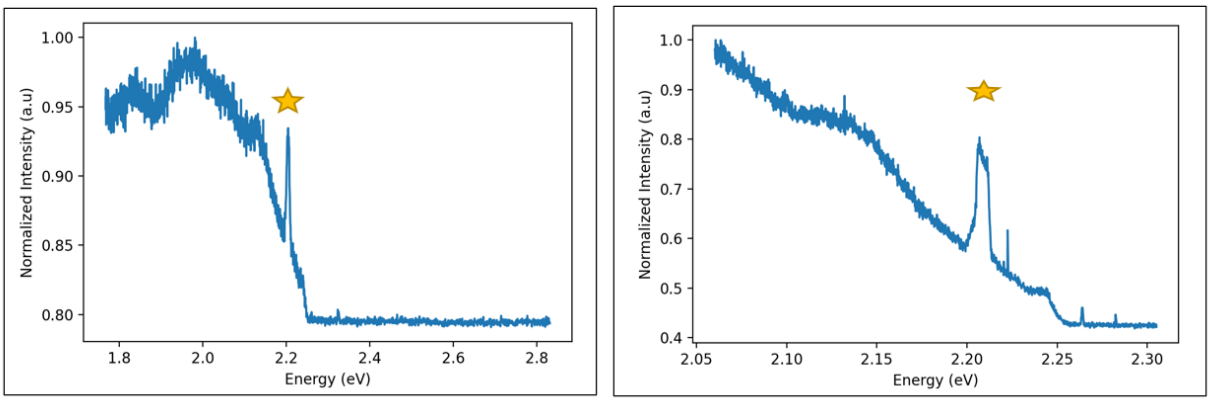

Figure 23: 4.K PL spectrum of low temperature annealed sample in the tylan9 deposited on SiN. The sharp peak located around 2.20 eV is somewhat promising for potential Rydberg excitons due to being in the right energy range and demonstrating narrow emission, as one would expect for Rydberg series emitters. Further investigation requires stronger crystal quality due to power broadening issues.

Ultimately, while the data demonstrates that we have successfully grown cuprite films, these growth results suggest a need for better crystalline quality microcrystals. So, while we can achieve high quality tenorite, or low quality cuprite, we need a secondary step to produce high quality cuprite microcrystals. We propose two such potential methods in the next section, but are open to considering other procedures like reactive sputtering or different annealing furnace environments.

Summary and Next Steps

Next Steps

In summary, we have achieved growth processes which can consistently produce high crystallinity CuO films, or lower crystallinity Cu_2O films. We characterized these samples using a large variety of techniques, including SEM, XRD, XPS, PL, and stress tests.

For our next steps, we aim to work towards the growth of high quality, microcrystalline Cu_2O. A few approaches we would like to explore include reducing microcrystalline CuO to Cu_2O, secondary anneals (sintering) of low quality Cu_2O material in hopes of promoting increased crystallinity and exploring reactive sputtering.

Reduction of CuO to Cu_2O has been demonstrated before in pure N_2 environments at least 850°C (San Pio, Martini, Gallucci, Roghair, & van Sint Annaland, 2018). One of the main challenges in these types of conversions is preventing the further reduction of Cu_2O into Cu, which can be managed by ensuring a pure N_2 environment. Furthermore, it is not explained in literature whether the crystalline structure of different phases of cuprous oxide is maintained through the reduction process. We hope to explore this type of process to better elucidate it and determine whether reduction is a feasible way to produce microcrystalline cuprite from microcrystalline tenorite.

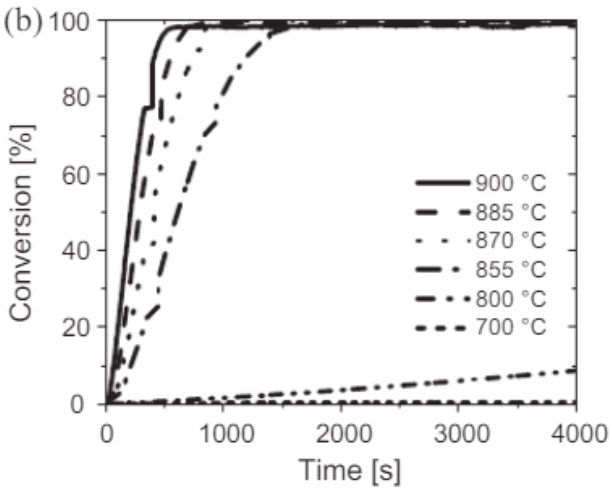

Figure 24: Conversion rates of tenorite into cuprite through an N_2 annealing reduction process for different annealing temperatures. We speculate that these conditions can be achieved in a secondary tylan9 anneal but need to explore the structure of cuprite produced via the reduction process. Adapted from San Pio, M.A et al.

Ultimately, we hope to integrate cuprite films with silicon nitride photonics and devices in order to conduct quantum and nonlinear optics experiments.

Benefits to the SNF community

We believe that our project contributes to the SNF's 'beyond silicon' initiative, as well as contributes to the community expertise on metal deposition, oxidation, and adhesion.

Appendices

Budget

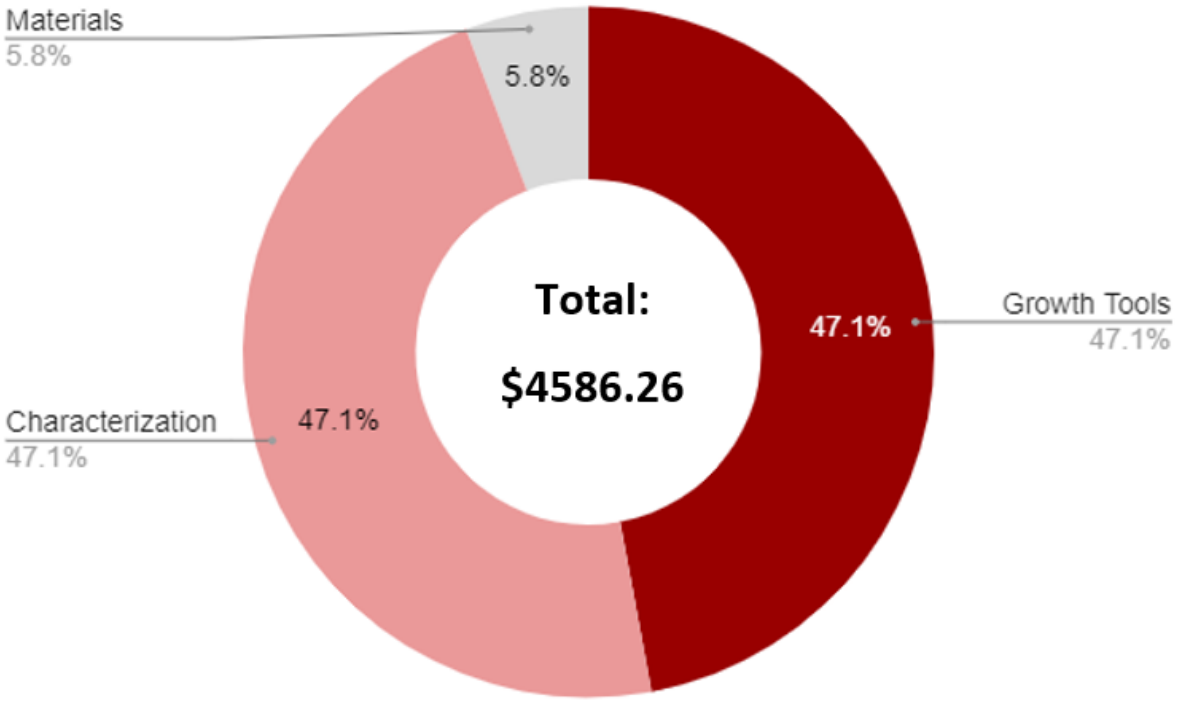

Figure 25: Summary of budget expenses throughout the quarter.

List of Samples

List of all samples and measurements done is attached at the end of the report.

References

Amekura, H., Plaksin, O. A., Kono, K., Takeda, Y., & Kishimoto, N. (2006). Production of Cu2O nanoparticles in SiO2 by ion implantation and two-step annealing at different oxygen pressures. *Journal of Physics D: Applied Physics*, *39*(16), 3659–3664. https://doi.org/10.1088/0022-3727/39/16/020

Choudhary, S., Sarma, J. V. N., & Gangopadhyay, S. (2016). Growth and characterization of single phase Cu2O by thermal oxidation of thin copper films. *AIP Conference Proceedings*, *1724*(April 2016). https://doi.org/10.1063/1.4945236

Choudhary, S., Sarma, J. V. N., Pande, S., Ababou-Girard, S., Turban, P., Lepine, B., & Gangopadhyay, S. (2018). Oxidation mechanism of thin Cu films: A gateway towards the formation of single oxide phase. *AIP Advances*, *8*(5). https://doi.org/10.1063/1.5028407

Flinn, P. A. (1991). Measurement and interpretation of stress in copper films as a function of thermal history. *Journal of Materials Research*, *6*(7), 1498–1501. https://doi.org/10.1557/JMR.1991.1498

Platzman, I., Brener, R., Haick, H., & Tannenbaum, R. (2008). Oxidation of polycrystalline copper thin films at ambient conditions. *Journal of Physical Chemistry C*, *112*(4), 1101–1108. https://doi.org/10.1021/jp076981k

Saffman, M., Walker, T. G., & Mølmer, K. (2010). Quantum information with Rydberg atoms. *Reviews of Modern Physics*, *82*(3), 2313–2363. https://doi.org/10.1103/RevModPhys.82.2313

San Pio, M. A., Martini, M., Gallucci, F., Roghair, I., & van Sint Annaland, M. (2018). Kinetics of CuO/SiO2 and CuO/Al2O3 oxygen carriers for chemical looping combustion. *Chemical Engineering Science*, *175*, 56–71. https://doi.org/10.1016/j.ces.2017.09.044

Scheel, S., Stolz, H., Bayer, M., Kazimierczuk, T., & Fro, D. (2014). *Giant Rydberg excitons in the copper oxide Cu 2 O*. 3–7. https://doi.org/10.1038/nature13832

Steinhauer, S., Versteegh, M. A. M., Gyger, S., Elshaari, A. W., Kunert, B., Mysyrowicz, A., & Zwiller, V. (2020). Rydberg excitons in Cu2O microcrystals grown on a silicon platform. *Communications Materials*, *1*(1), 3–8. https://doi.org/10.1038/s43246-020-0013-6

Substrate/ Stack	Oxidation Tool	Oxidation Parameters	SEM	XPS	XRD	PL	Other Notes
Cu 200/Si	Thermolyne	300C 1hr	yes	Cu2p	Cu2O	Weak RT, Defect dominated Cryo	
Cu 200/Ti 5/Si	Thermolyne	300C 1hr	yes				
Cu 200/Si	Thermolyne	300C 3hr	yes				
Cu 200/Ti 5/Si	Thermolyne	300C 3hr	yes				
Cu 200/Si	Thermolyne	800C 1hr	yes				
Cu 200/Ti 5/Si	Thermolyne	800C 1hr	yes				
Cu 200/Si	Thermolyne	800C 3hr	yes				
Cu 200/Ti 5/Si	Thermolyne	800C 3hr	yes				
Cu 200/Si	Tylan9	800C 3hr	yes				
Cu 200/Ti 5/ Si	Tylan9	800C 3hr	yes				
Cu 700/Ti 5/Si	Tylan9	800C 3hr	yes				
Cu 700/Ta 5/Si	Tylan9	800C 3hr	yes	survey, HR, depth, post sputter Cu2p			sample with the cleanest microcrystals observed
Cu 700/Ti 5/SiN	Tylan9	800C 3hr					
Cu 200/Si	Tylan9	800C 1hr	yes				
Cu 200/Ti 5/ Si	Tylan9	800C 1hr					
Cu 700/Ti 5/Si	Tylan9	800C 1hr					
Cu 700/Ta 5/Si	Tylan9	800C 1hr	yes				
Cu 700/Ti 5/SiN	Tylan9	800C 1hr					
Cu 200/Si	Tylan9	300C 3hr	yes				
Cu 200/Ti 5/ Si	Tylan9	300C 3hr					
Cu 700/Ti 5/Si	Tylan9	300C 3hr					
Cu 700/Ta 5/Si	Tylan9	300C 3hr	yes				
Cu 700/Ti 5/SiN	Tylan9	300C 3h	yes				
Cu 200/Si	Tylan9	300C 1hr	yes (peel)	survey, Cu2p, Cu LMM, post sputter Cu2p, post sputter Cu LMM, post sputter O			
Cu 200/Ti 5/ Si	Tylan9	300C 1hr					
Cu 700/Ti 5/Si	Tylan9	300C 1hr					
Cu 700/Ta 5/Si	Tylan9	300C 1hr	yes				
Cu 700/Ti 5/SiN	Tylan9	300C 1hr	(peel)		Cu2O XRD	Interesting Cryo PL	
Cu 200/Si	Lesker	700C 1hr	yes				
Cu 700/Ta 5/Si	Lesker	700C 1hr	yes	survey, depth, post sputter Cu2p/CuLMM/O			
Cu 700/Ti 5/Si	Lesker	700C 1hr	yes				
Cu 700/Ti 5/SiN	Lesker	700C 1hr	yes	survey, depth, post sputter Cu2p/CuLMM/O			
Cu 200/Ti 5/Si	Tylan9	25OX1000	yes				
Cu 700/Ti 5/Si	Tylan9	25OX1000	yes				
Cu 700/Ta 5/Si	Tylan9	25OX1000	yes	survey, all HR +fits			
Cu 200/Ti 5/Si	Tylan9	15OX1000					
Cu 700/Ti 5/Si	Tylan9	15OX1001					
Cu 700/Ta 5/Si	Tylan9	15OX1002					
Cu 200/Ti 5/Si	Tylan9	5OX1000					
Cu 700/Ti 5/Si	Tylan9	5OX1001					
Cu 700/Ta 5/Si	Tylan9	5OX1002	yes				
Cu 700/Ti 5/Si	Lesker	05/05/2021 parameters	yes	survey, all HR+fits, depth (w sputter problems)/ 2nd survey, all HR+fits, depth			
Cu 700/Ti 5/Si	Lesker+Thermolyne	05/05/2021 parameters+250C 24hr	yes	survey, all HR+fits, depth			
Cu 700/Ta 5/Si	Thermolyne	250C 24hr	yes				
Cu 700/Ti 5/Si	Thermolyne	250C 24hr	yes	survey, all HR+fits			potentially cuprite, just lumpy :(
Cu 700/Ti 5/SiN	Thermolyne	250C 24hr	yes				

	Cu Reference	None	None	yes	survey, HR, post sputter HR					
	Cu 700/Ti 5/Si 1	Tylan9	300C 1hr	yes						
	Cu 700/Ti 5/Si 2	Tylan9	300C 1hr	peel						
	Cu 700/Ti 5/Si 3	Tylan9	300C 1hr	peel						
	Cu700/Ta 5/Si 1	Tylan9	300C 1hr	yes						
	Cu700/Ta 5/Si 2	Tylan9	300C 1hr	yes						
	Cu700/Ta 5/Si 3	Tylan9	300C 1hr	peel						
	Cu700/ Ti 5/SiN 1	Tylan9	300C 1hr	yes						
	Cu700/ Ti 5/SiN 2	Tylan9	300C 1hr	yes						
	Cu700/ Ti 5/SiN 3	Tylan9	300C 1hr	yes						